Exploring Bipedal Hopping through Computational Evolution

Jared M. Moore*
Grand Valley State University
School of Computing and Information Systems
moorejar@gvsu.edu

Catherine L. Shine
Hartpury College
Department of Animal Science

Craig P. McGowan
University of Idaho
Department of Biological Sciences

Philip K. McKinley
Michigan State University
Department of Computer Science and Engineering

Abstract Bipedal hopping is an efficient form of locomotion, yet it remains relatively rare in the natural world. Previous research has suggested that the tail balances the angular momentum of the legs to produce steady state bipedal hopping. In this study, we employ a 3D physics simulation engine to optimize gaits for an animat whose control and morphological characteristics are subject to computational evolution, which emulates properties of natural evolution. Results indicate that the order of gene fixation during the evolutionary process influences whether a bipedal hopping or quadrupedal bounding gait emerges. Furthermore, we found that in the most effective bipedal hoppers the tail balances the angular momentum of the torso, rather than the legs as previously thought. Finally, there appears to be a specific range of tail masses, as a proportion of total body mass, wherein the most effective bipedal hoppers evolve.

Keywords
Evolutionary robotics, bipedal hopping, biomechanics, genetic algorithm, gait analysis

1 Introduction

Bipedal hopping has evolved in relatively few mammalian species [15]. In large animals, such as kangaroos and wallabies, hopping is an efficient gait exploiting mechanical properties of the large tendons in the lower legs [1, 4]. In smaller animals, such as springhares, jerboas, and kangaroo rats, hopping is used primarily as a predator escape mechanism [3]. Despite the large disparity in size among these species, however, they all exhibit common morphological characteristics, namely large, powerful rear legs combined with relatively long tails.

Tails have been shown to play an important role in locomotion in many animals, for example, assisting in the control of body orientation and helping to stabilize gaits [13, 14]. Studies of the tail with respect to bipedal hopping, as well as the evolutionary origins of this behavior, have been relatively few, perhaps due to the limited number of species that exhibit it. Alexander and Vernon investigated the musculoskeletal system of kangaroos and described the mechanics of movement during locomotion [1], hypothesizing that the tail balances the angular momentum produced by the swinging of the rear legs. This result was supported by analyzing bipedal hopping of multiple kangaroo species [2]. Usherwood and Hubel [19] also evaluated kangaroo gaits and concluded that, aside from increasing stability, the long-tail–long-head morphology of kangaroos may help to reduce the energetic cost of locomotion in bipedal hopping.

* Corresponding author.

A complementary approach to studying basic questions in evolutionary biology is *computational evolution* [6, 17], which enables exploration of evolutionary paths beyond those followed by extant species. When applying this method to study animal behavior, digital genomes encode the morphological and control parameters of *animats* [20]. Populations of animats are subject to evolutionary pressures in addressing tasks such as locomotion, with performance evaluated in a physics-based simulator. The resulting morphologies and controllers, along with their lineages, can be analyzed to help identify the salient factors in the evolution of particular behaviors [5, 7, 8, 12].

Hase et al. [10] applied this approach to two-dimensional (2D) animats with simulated neuromuscular morphologies, demonstrating bipedal and quadrupedal hopping gaits reminiscent of those observed in nature. More recently, Moore et al. [16] conducted a study in the evolution of bipedal hopping in three-dimensional (3D) animats, where object masses and the forces applied to them are integral to the evolution of stable and effective gaits. That study showed that a tail is essential to hopping, but that different morphologies can lead to very different gaits, some resembling those of biological organisms and others not observed in any known species. The most effective bipedal hopping gaits exhibited a close coupling between tail movement and the oscillation frequency of leg joints. However, that study did not address the evolutionary origins of hopping.

In this study, we evolve 3D animats in order to elucidate what morphological and control characteristics lead to the evolution of bipedal hopping. Animats are evaluated based on their distance traveled in a fixed period of time on a flat, high-friction surface. In the experiments, we observe the evolution of both bipedal hopping and bounding gaits. Analysis of the gaits and evolutionary trajectories yields the following contributions. First, we assess the performance of bipedal hopping versus bounding for morphologies with fixed tail characteristics. Second, we determine which genes lead to bipedal hopping or bounding behaviors, by examining the evolutionary history of individual runs. Finally, we analyze the relationship between angular momentum and the phase of the rear legs, torso, and tail in evolved animats.

2 Methods

2.1 Animat and Simulation Environment

Figure 1 shows the initial simulated animat, which is based on the dimensions and masses of a desert kangaroo rat (*Dipodomis deserti*). The animat comprises 19 components: 3-segment torso, head, 3-segment tail, 4-segment rear legs, and 2-segment forelimbs. As described below, the physical properties of these components, as well as the control properties of their movements, are allowed to evolve.

Evaluations conducted as part of the evolutionary algorithm are implemented in the Open Dynamics Engine (ODE) [18], a three-dimensional real-time physics simulator. The ODE provides an

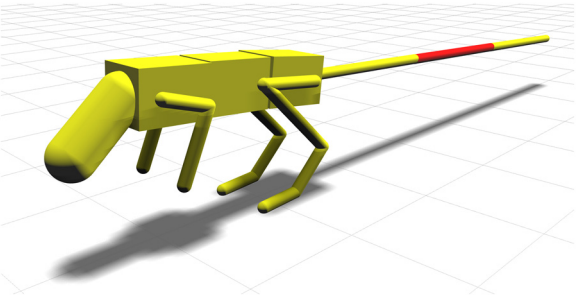

Figure 1. The hopping animat used in this study in the 3D physics simulation environment. Morphological characteristics are based on a kangaroo rat (*D. deserti*). Note: the middle segment of the tail is colored red to illustrate the three sections of the tail.

environment to simulate an animat with components connected by actuated joints. It handles collisions between components, as well as modeling forces such as friction and gravity. Each evaluation is conducted for 10 s of simulation time and divided into discrete time steps of 0.005 s. For each time step, the state of the animat is updated using standard physics equations. When two components come into contact with each other, their mass, velocity, dimensions, and friction coefficients are taken into account with appropriate forces applied to each body, producing physically realistic reactions.

Components are connected by either actively controlled or passive joints. Actively controlled joints are similar to animal joints governed by muscles, while passive joints more closely model spring systems such as tendons. In this article, we employ power-limited hinge joints with defined ranges of motion. Movement of limbs is achieved by specifying a velocity for each active joint per time step. If the forces acting upon a joint exceed the maximum output power, the joint flexes, allowing for smooth interaction between animat and the surrounding environment.

Table 1. Components of the animat's genome.

Gene	Description
	Morphology Genes
Posterior_Torso_Mass	Posterior torso segment mass
Mid_Torso_Mass	Middle torso segment mass
Anterior_Torso_Mass	Anterior torso segment mass
Tail_Len	Length of the tail
RH_MF	Hip maximum joint force
RK_MF	Knee maximum joint force
RA_MF	Ankle maximum joint force
RT_MF	Toe maximum joint force
FS_MF	Shoulder maximum joint force
FE_MF	Elbow maximum joint force
T_MF	Tail maximum joint force
	Control Genes
Max_Joint_Vel	Maximum joint velocity
Osc_Freq	Oscillation frequency for controller
RRL_Off	Right-rear-leg oscillating-signal phase offset
LRL_Off	Left-rear-leg oscillating-signal phase offset
RFL_Off	Right-front-leg oscillating-signal phase offset
LFL_Off	Left-front-leg oscillating-signal phase offset
RH_Off	Hip oscillating-signal phase offset
RK_Off	Knee oscillating-signal phase offset
RA_Off	Ankle oscillating-signal phase offset
RT_Off	Toe oscillating-signal phase offset
FS_Off	Shoulder oscillating-signal phase offset
FE_Off	Elbow oscillating-signal phase offset
T_Off	Tail oscillating-signal phase offset
TB_Off	Tail-base oscillating-signal phase offset

2.2 Evolutionary Algorithm

Computational evolution draws from biological evolution, solving problems in scientific and engineering domains [9]. Here, we apply a generational genetic algorithm (GA) [11] as follows. The GA operates on a population of 120 animat genomes that evolve for 2,000 generations. An individual's fitness is defined as the forward (the head defines the front of the animat) Euclidean distance traveled over 10 s of simulation time. The algorithm uses two-way tournament selection, wherein two parents are selected from the population. Each child has a 50% chance of being a clone of the parent with the higher fitness, and a 50% chance of being a combination of both parents through crossover. Finally, mutation is applied to the child genome with a 5% chance per gene. If a gene is mutated, the new value is chosen randomly from a Gaussian function whose mean μ is equal to the gene's current value and whose parameter σ is equal to 10% of the gene's allowed range. We conduct 20 replicate runs per treatment, each initialized with a unique random number seed, enabling search of different evolutionary paths.

2.3 Genome

An individual is codified by a genome consisting of parameters that define both morphology and control. Table 1 lists the genes and a brief description of each. The first three genes, *Rear_Torso_Mass*, *Mid_Torso_Mass*, and *Front_Torso_Mass*, define the masses of the torso segments. *Tail_Len* allows the length of the tail to evolve up to a maximum of 1.86 body lengths. Parameters denoted as *xx_MF* define the maximum force output that can be exerted during actuation by the indicated joint. The remaining parameters are associated with control of the animat. *Max_Joint_Vel* sets the maximum angular velocity of the hinge joints. *Osc_Freq* specifies the common oscillating frequency that drives all joints. The next four parameters (*RRL_Off*, *LRL_Off*, *RFL_Off*, and *LFL_Off*) define the phase offset per leg. A phase offset modifies the timing of the oscillating signal, enabling each leg to move in a different phase. The phase offset for a leg applies to all joints in that limb. For example, *RRL_Off* applies the offset to the hip, knee, ankle, and toe joints of the right rear leg. The next eight parameters (*RH_Off*, *RK_Off*, *RA_Off*, *RT_Off*, *FS_Off*, *FE_Off*, *T_Off*, and *TB_Off*) define offsets for corresponding pairs of joints. For example, *RH_Off* defines a phase offset for both left and right hip joints. Together, the leg and joint offsets allow for synchronous or asynchronous coordination among limbs while being driven by the same oscillating signal (e.g., the two rear legs can exhibit the same cyclic motion, but in different phases).

2.4 Treatments

Table 2 lists the eight treatments in this study. In the first part of our study, we conduct six treatments, each with a different tail mass. These fixed mass (FM) treatments set the total tail mass as a

Table 2. List of treatments.

Abbreviation	Treatment
FM-2.5%	Fixed tail mass 2.5%
FM-4.9%	Fixed tail mass 4.9%
FM-9.3%	Fixed tail mass 9.3%
FM-17%	Fixed tail mass 17%
FM-23.5%	Fixed tail mass 23.5%
FM-38.1%	Fixed tail mass 38.1%
ELM-3%	Evolvable length and mass 3%
ELM-13.3%	Evolvable length and mass 13.3%

percentage of total body mass (2.5%, 4.9%, 9.3%, 17%, 23.5%, and 38.1%), with the mass being distributed equally among the three tail segments. The other components of the animat's morphology, including dimensions and torso and limb masses, remain fixed.

In the second set of treatments, the masses of the tail segments are also allowed to evolve. These evolvable-length–mass (ELM) treatments expand the space of possible body configurations beyond those in the FM treatments. Two treatments are conducted with a minimum tail mass of 3% of body mass (ELM-3%) and 13.3% of body mass (ELM-13.3%).

2.5 Gait Classification and Analysis

Bipedal hopping and bounding are the two primary gaits that evolve in this study. Behaviors are classified by selecting the farthest-traveling individual in each replicate and visually observing its gait. Bipedal hopping is defined as a repeating cyclic gait where the rear legs move synchronously, providing forces required to support stance and propulsion during locomotion. A single bipedal hopping gait cycle is shown in Figure 2(a). The animat has a stable body position throughout the hopping movement. Locomotion is driven by the rear legs with the tail balancing the pitch of the body. Bounding is characterized by the hind and fore limbs alternating contact with the ground. A bounding gait cycle is shown in Figure 2(b).

When analyzing a gait, we consider the center of mass (COM), relative phase of limb movements, and angular momentum. For evaluation, the animat is considered as three composite sections (rear legs, tail, and torso). The torso section is composed of the three torso segments as well as the head. Movement of a section is quantified by measuring the COM about the reference point located at the hip. A section's COM is calculated as the average (x, y) position across the components of the section. The anterior-posterior axis is x, and the height above the ground is y. The side-to-side axis (z) remains constant, as left-right symmetry is enforced in the animat. The movement phase for each section is calculated by measuring the oscillation of the COM about the reference point. Phase is derived by sampling the angle between a component's COM and reference point at each time step and then applying the Hilbert transformation. We use the hip as the reference point to measure angular momentum. At each time step, the angular momentum of a segment is calculated by multiplying the moment of inertia by the angular velocity of that segment about the hip.

2.6 Genome Analysis

For each replicate run, we compile a list of the farthest-traveling individuals over evolutionary time. The list is constructed as follows: Beginning with the first generation's population, we select the farthest-traveling individual and add it to the list. For each subsequent generation, if an individual traveled farther than the individual previously added, we append the new farthest-traveling individual

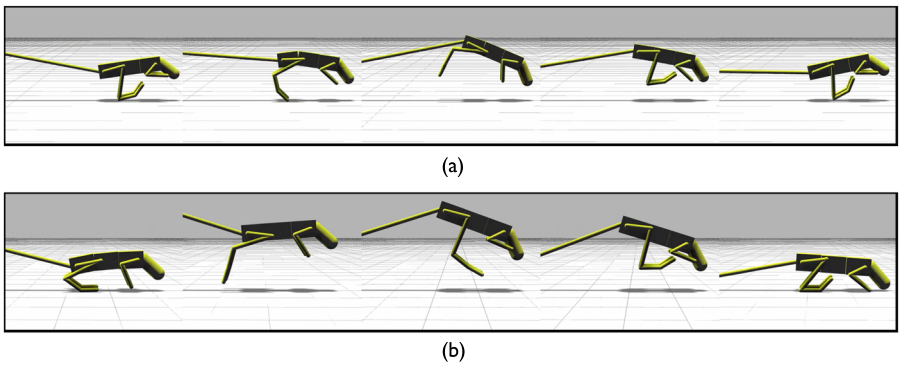

Figure 2. Representative bipedal hopping and bounding gaits. (a) A single hopping cycle. Note that the rear legs drive locomotion with no ground contact for the forelimbs or head. (b) A single bounding cycle from a representative individual. Note that the forelimbs contact the ground.

with the list. This process produces a list of intermediate individuals (i.e., individuals who were at one time the farthest-traveling), ending with the farthest-traveling individual over the entire run. Gene fixation is determined by comparing the genome for each intermediate individual with that of the farthest-traveling individual per replicate. The difference for each gene is calculated and normalized to the range of values of that gene.

3 Results

3.1 Behavior and Distance Traveled

Bipedal hopping evolved in five of the six FM tail treatments, although bounding is the most common behavior. Other locomotion strategies evolved in 9 of the 120 replicate runs, but we do not include them in our analysis, as they were unstable movements. A video of evolved results is available at https://youtube/2JvlChVJQEE.

Figure 3 plots the behavior versus distance traveled for the best individual per replicate across the FM treatments. In all cases, bipedal hoppers travel farther than bounding individuals. The farthest-traveling bipedal hoppers have tail masses of 9.3% and 17% of total body mass. For tail masses above 17%, the total number of bipedal hoppers drops off considerably, with none evolving in the FM-38.1% treatment. The average distance traveled by bounding individuals decreases as tail mass increases.

3.2 Evolutionary Paths to Bipedal Hopping and Bounding

Figures 4(a) and 4(b) plot the average genetic distance for bipedal hoppers and bounders, respectively, over evolutionary time. The *y*-axis is normalized to a range of [0, 1], with 0 representing the first individual and 1 representing the farthest-traveling individual, averaged across the 20 replicates. The level of shading of a cell is proportional to the average genetic distance between the intermediate and the final individual across replicates. Darker cells represent genes that have high variability, and lighter shading represents genes that have fixated. For example, in Figure 4(a), the *RH_Off* column is lightly shaded. This gene fixates early, enabling the rear-leg-driven gait. In contrast, the *FS_MF* gene is darkly shaded up the entire column, indicating that the gene varies considerably over

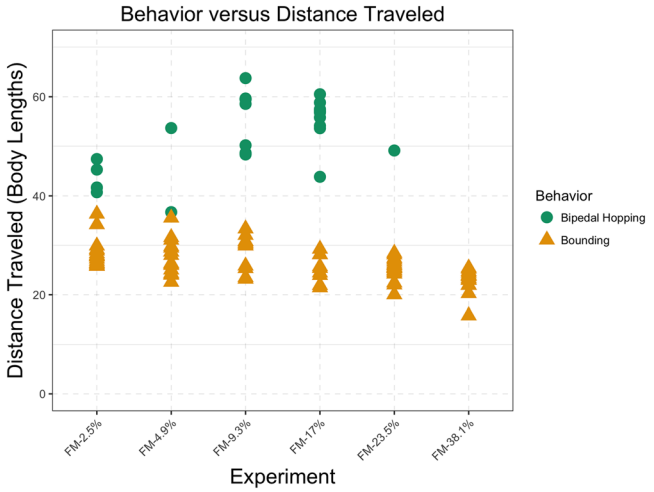

Figure 3. Behavior versus distance traveled for the farthest-traveling individual across the FM treatments. Each treatment comprises 20 replicate runs. Only replicates that produce bipedal hopping and bounding behaviors are included in this figure.

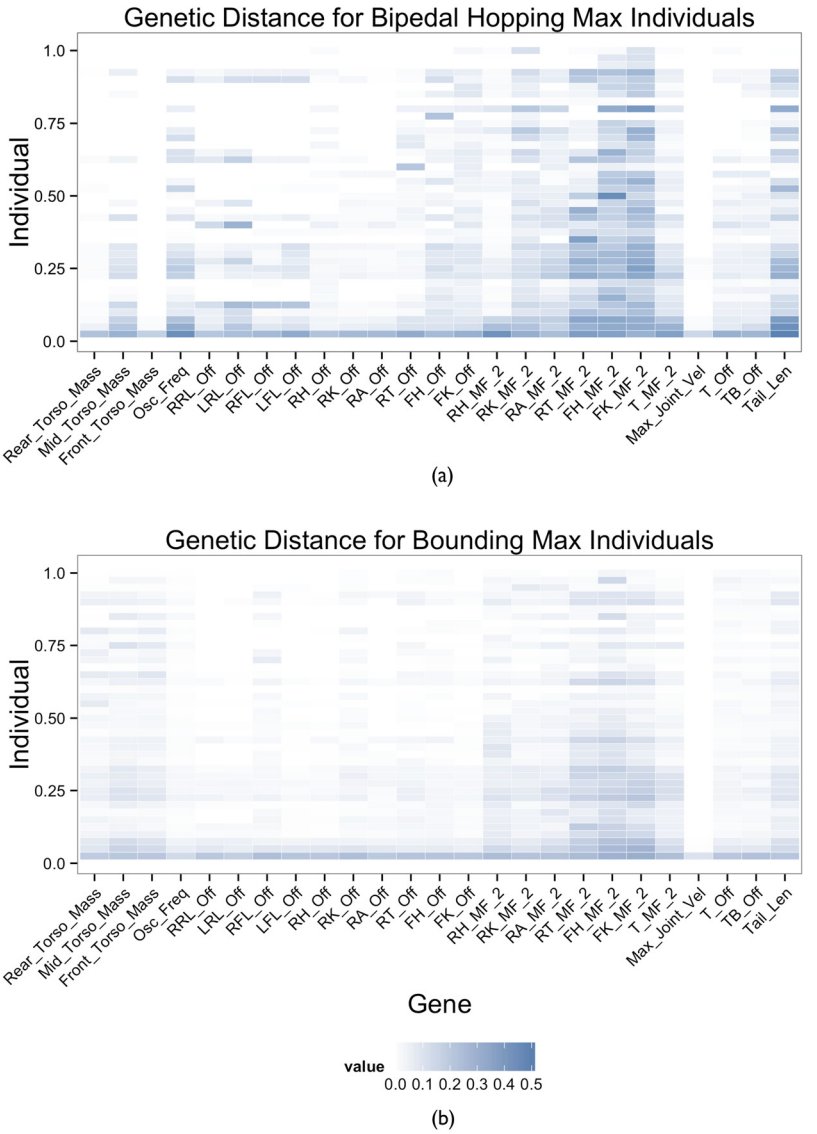

Figure 4. Genetic distance for (a) bipedal hoppers and (b) bounders across the replicate runs. Darker shades indicate values that are farther away from the final individual. Columns with light shading indicate genes that fixate early in a run.

evolutionary time. This gene defines the maximum force the shoulder joint can output, which does not drive the bipedal hopping gait.

Comparing Figures 4(a) and 4(b), we find several key differences, as well as similarities, in the evolution of hoppers and bounders. Joint maximum forces in the limbs vary in both hoppers and bounders over evolutionary time. In hoppers, the front limbs vary considerably, as indicated by the darker shading in columns *FS_Off* and *FE_Off*. Joints in the front limbs are under less selective pressure due to the bipedal hopping gait's utilization of the rear limbs to drive locomotion. Torso masses (*_*Torso_Mass*) stabilize fairly early for bipedal hoppers, whereas bounders exhibit varying torso masses over time. Given the stability of the bounding gait, changes in torso mass likely have

less effect on performance than for bipedal hoppers, where controlling pitch momentum is essential. A high degree of torso mass variability would likely produce unstable hopping gaits. Furthermore, we observe that the leg joint phase offsets (*RRL_Off*, *LRL_Off*, *RFL_Off*, *LFL_Off*) stabilize early for bounders, while the genes in bipedal hoppers continue to evolve up until the most effective individual. Due to the highly coordinated bipedal hopping gait, requiring synchronization of limbs and tail, along with balanced masses, it appears to take longer for evolution to produce a stable gait. Finally, we note that the tail length varies in both bounders and bipedal hoppers, but more so in bipedal hoppers. We speculate that this characteristic is due to the balance between tail and torso movement needed to realize effective bipedal hopping.

3.3 Phase and Angular Momentum

Figure 5 plots the angular momentum of the rear legs, tail, and torso for the bipedal hopper in Figure 2(a), the farthest-traveling individual across all treatments. The tail and torso data have been scaled down by two orders of magnitude in order to show the relationship between the three components. Considering the scaling, the tail and torso account for almost all angular momentum in the animat. Moreover, the tail and torso cancel the angular momentum of each other, with a measured phase difference of 0.99π, allowing for a stable body posture during locomotion.

Figures 6(a), 6(b), and 6(c), respectively, plot the pairwise phase differences between torso, tail, and rear legs of the farthest-traveling individual in each replicate run. For bipedal hoppers, these evolved phase differences tend to fall within a relatively small range of values. Bipedal hopping requires coordination between torso, tail, and rear legs to balance the animat during movement. In contrast, phase differences for bounders tend to vary widely, as coordination between the various components is not as crucial.

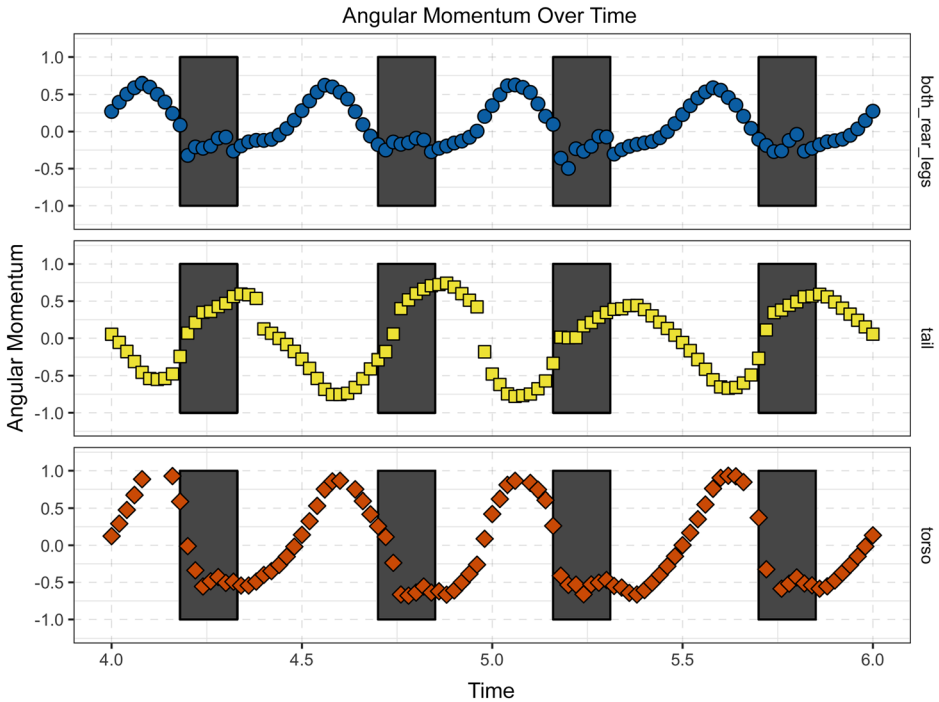

Figure 5. Angular momentum for the rear legs, tail, and torso of the farthest-traveling individual from the FM-9.3% treatment between 4.0 and 9.0 s of simulation time. The tail and torso have been scaled down by two orders of magnitude to be in line with the rear legs. Shaded boxes indicate the ground contact phase of the gait.

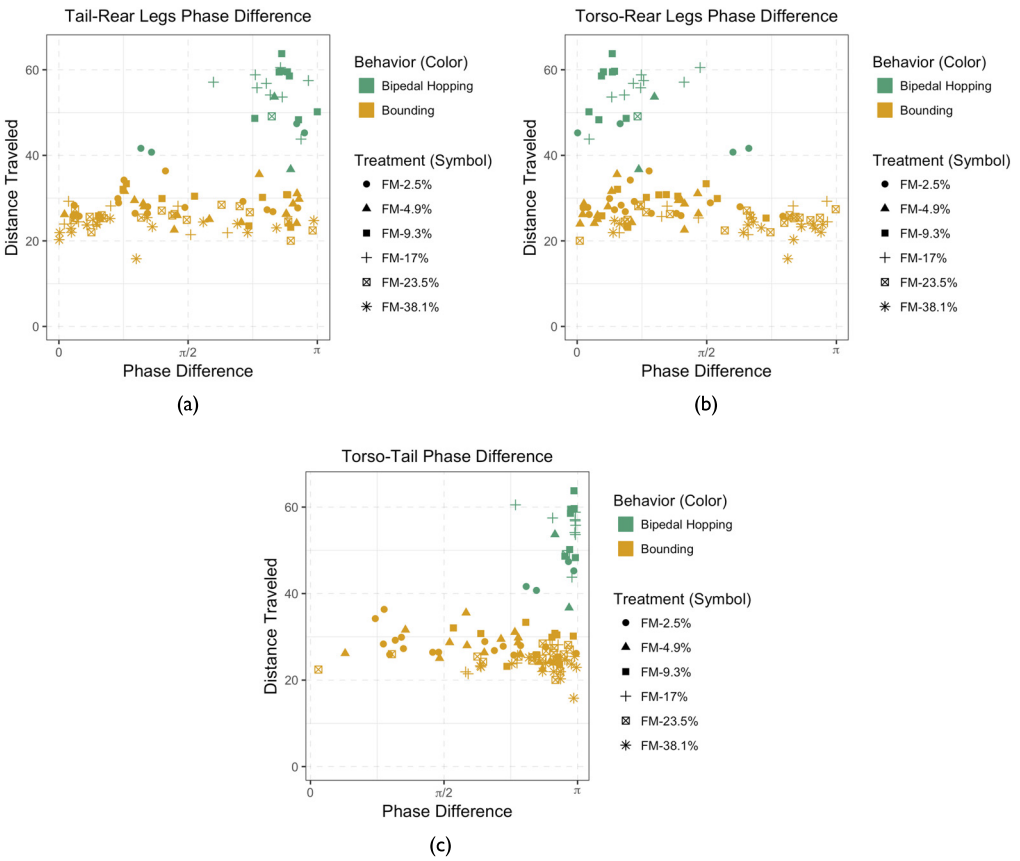

Figure 6. Phase difference between (a) tail and rear legs, (b) torso and rear legs, and (c) tail and torso for the farthest-traveling-individual per replicate across the FM treatments.

As shown in Figure 5, the tail moves against the torso (high mass) and rear legs (low mass), countering the angular momentum of the two components. This leads to the out-of-phase movement indicated in Figures 6(a) and 6(c). Due to the high mass of the torso, phase offsets between the tail and torso are nearly out of phase, as seen in Figure 6(c). On the other hand, the torso and rear legs move almost in phase, together moving against the tail; see Figure 6(b). However, we note that the phase difference is not 0, since movement in the rear legs drives pitch change in the torso.

Figure 7(a) plots the total angular momentum for the farthest-traveling individual in each replicate run. We sample between 4.0 and 9.0 s to measure the stable phase of gaits, avoiding bias from the transient phases at the start and end of a simulation. A total angular momentum near 0 indicates a stable gait cycle, whereas high angular momentum values are typically associated with unsteady gaits. The angular momentum values have a slight bias above 0, as we measure from the rear hip for consistency, since the center of mass changes due to evolution of the animats. The farthest-traveling bipedal hoppers and bounders have a net angular momentum near 0. Figure 7(b) plots the distance traveled versus the angular momentum of the combined torso and tail components. Again, the most effective bipedal hoppers (and to a lesser degree bounders) have a net angular momentum near 0, as the tail and torso move out of phase with each other, countering body pitch; see Figures 2(a) and 6(c).

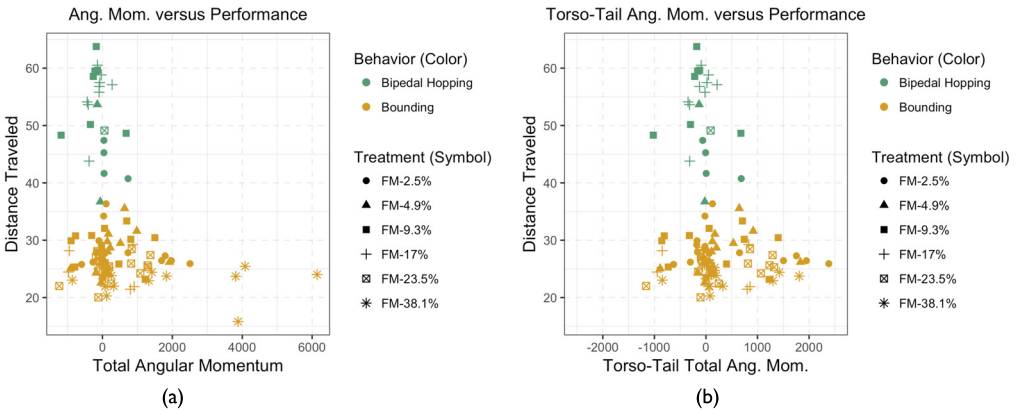

Figure 7. (a) Total angular momentum (4.0 to 9.0 s of simulation time) versus distance traveled for the farthest-traveling individual per replicate in the FM treatments. (b) Torso and tail total angular momentum (4.0 to 9.0 s of simulation time) versus distance traveled.

Figure 8(a) plots the tail mass as a percentage of total body mass versus distance traveled for the FM treatments. The farthest-traveling hoppers have a tail mass in the range of 8% to 18% of the total body mass. Figure 8(b) plots the torso masses of the farthest-traveling individual from each replicate run. All evolved bipedal hoppers have torso masses from 0.9 to 2.1 units, with the farthest-traveling bipedal hopper having a body mass of approximately 1.4 units. This result suggests the possibility of an optimal torso and tail mass combination for bipedal hopping.

3.4 Evolvable Tail Mass and Tail Length

We next conduct two treatments where the tail mass is an evolvable parameter. Figures 9(a) and 9(b) plot the tail mass as a percentage of total body mass versus distance traveled and the tail length versus distance traveled, respectively, for the two ELM treatments. The first treatment, ELM-3%, places a minimum constraint of 3% of initial starting total body mass in the tail (1% for each of the three segments). Three of the 20 replicates (green circles) exhibit bipedal hopping, and all three have evolved relatively high tail mass. A second treatment (ELM-13.3%) increases the minimum tail

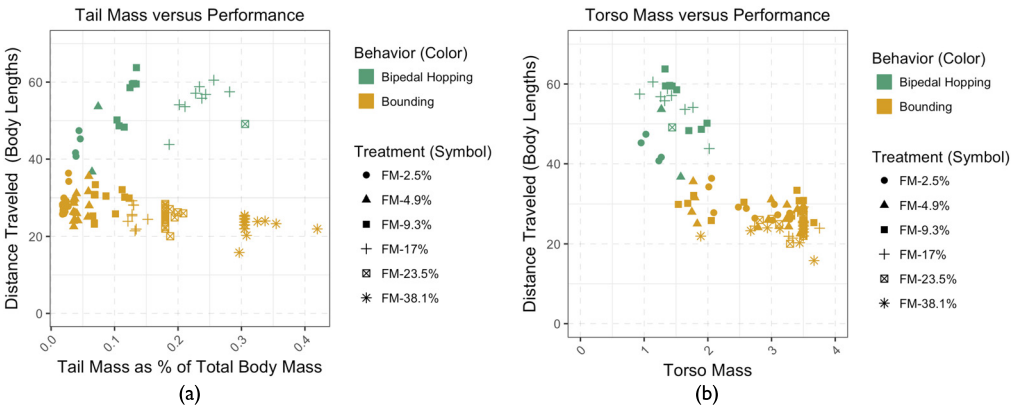

Figure 8. (a) Tail mass as a proportion of total body mass for the FM treatments. (b) Torso (including head) mass for the farthest-traveling individual per replicate across the FM treatments.

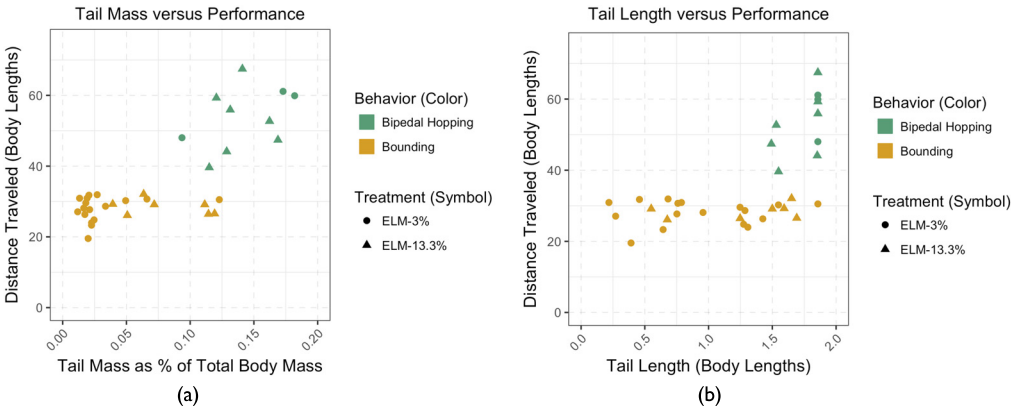

Figure 9. (a) Tail mass as a percentage of total body mass versus performance for the two ELM treatments. (b) Tail length versus distance traveled for the ELM treatments.

mass to 13.3% of initial total body mass (4.9% per segment). In this treatment, 7 of the 20 replicates (green triangles) evolve bipedal hopping. The farthest-traveling individual reaches a distance of 67.49 body lengths. We note that the tails of the farthest-traveling hoppers in these two treatments range from 12% to 18% of total body mass, similarly to the FM treatments. The percentages for the two ELM treatments are calculated based on the starting mass of the animat. In general, bipedal hoppers tend to exhibit heavier and longer tails than bounders. The longer tails and high tail mass allow the bipedal hoppers to counter the pitching of the torso as the rear legs move, producing the stable body posture needed for fast bipedal hopping.

Figure 10(a) plots the torso mass distribution versus tail mass distribution for the ELM treatments. For bipedal hoppers, the torso mass distribution is similar to that of the FM treatments, with the weight being distributed toward the front of the torso. In comparison with bounders, the torso mass is generally biased towards the front of the animat, while the tail mass is farther to the rear. Along with the longer tail length and rearward tail mass distribution (see Figure 10(b)), this allows the bipedal hoppers to have longer moment arms for the tail and torso, balancing the angular momentum between the two components. The characteristics of the tail appear to be less important for bounding, in view of the higher variance exhibited in the two plots.

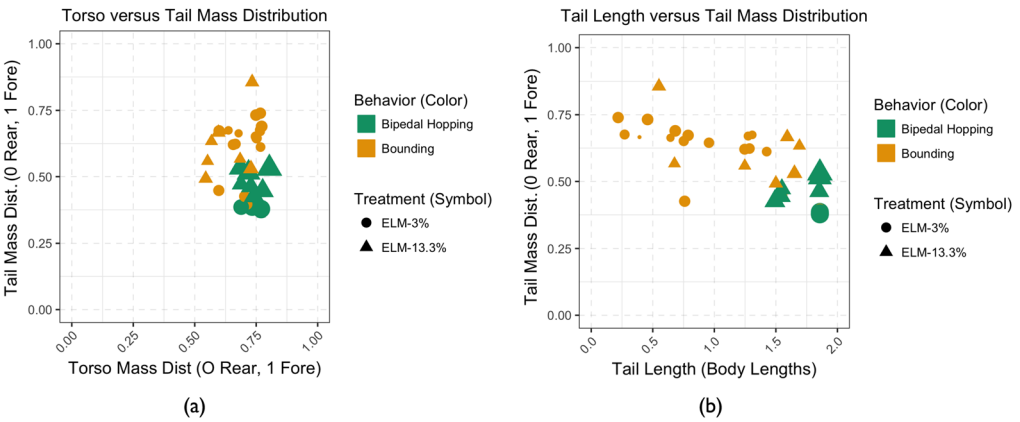

Figure 10. (a) Torso versus tail mass distribution for the ELM treatments. (b) Tail length versus tail mass distribution for the ELM treatments. Point size is proportional to the distance traveled.

4 Discussion

In this study, we have explored the evolution of bipedal hopping in an animat whose initial morphology is based on the kangaroo rat. Among the 160 evolutionary runs, bounding gaits emerge more frequently than hopping, likely due to the relative stability provided by four limbs coming in contact with the substrate. However, bounders also exhibit a relatively high variance in morphological characteristics and distance traveled.

In contrast, the morphologies of bipedal hoppers converge, exhibiting relatively long tails and mass distributed toward the front of the torso. Behaviorally, bipedal hopping is aided by movement of the tail, which is raised during the power stroke in the rear legs and lowered while the legs recover. Body pitch is conserved, resulting in a stable, level torso. As a result, the bipedal hoppers travel significantly farther than their bounding counterparts. When tail mass and tail mass distribution are included as evolvable parameters, bipedal hoppers evolve heavier tails with mass distributed toward the distal end, producing the highest-performing individuals observed across all treatments.

We presumed that bipedal hopping would evolve from bounding, since the latter is generally a more stable form of locomotion. Instead, we find that the two behaviors are divergent, with the farthest-traveling individuals in each replicate exhibiting one or the other behavior early in the evolutionary process. Examining the genomes of farthest-traveling individuals over evolutionary time, we find that left-right symmetry, low torso masses, and hip strength are key factors in the emergence of bipedal hopping. Early fixation of the corresponding genes is evident in bipedal hoppers, whereas in bounders those gene values vary over evolutionary time.

The evolved hopping gaits demonstrate coordination between the phase of movement and angular momentum of the tail, torso, and rear legs. Genetically, it appears that changes in phase occur simultaneously at the limb or the joint level, maintaining symmetric movement between limbs. Simultaneous change can be seen in Figure 4(a), where the limb level phase offsets (*RRL_Off*, *LRL_Off*) vary together. The evolution of phase offsets among tail, torso, and rear limbs results in the torso and tail moving against each other during locomotion. The pivot point of the gait is located near the hip, reducing the pitching moment of the animat. In the most effective bipedal hoppers, the rear legs and tail (Figure 6(a)) and the tail and torso (Figure 6(c)) are approximately out of phase with one another (i.e., phase difference close to π), while the hind limbs and torso (Figure 6(b)) move nearly in phase.

This relationship is also seen in natural organisms. Alexander and Vernon [1] studied kangaroos and suggest that the tail balances the angular momentum of the legs, thus reducing the pitching effect produced by hip rotation during locomotion. However, in our evolved animats the tail primarily serves to balance the angular momentum of the torso, and the farthest-traveling bipedal hoppers have a net angular momentum near 0 (Figure 7(b)). Furthermore, the rear legs produce angular momentum values two orders of magnitude less than the torso and tail. Therefore, in this study, where computational evolution allows us to trace lineages and relationships among genes, it appears that balancing the angular momentum of the torso and tail is more important than balancing the legs and tail.

5 Conclusions and Future Work

Bipedal hopping is a relatively rare, yet effective form of locomotion in animals. It can be difficult to study in biological organisms, given the low number of species exhibiting the behavior and limitations of physical observation. Here, we employ computational evolution and a digital physics simulation to study which morphological control factors enable bipedal hopping. Specifically, we investigate the differences between bipedal hopping and bounding for an animat initially based on a kangaroo rat. Across six treatments, we find that bipedal hopping and bounding are divergent behaviors with key genetic differences arising early in evolution. Second, the tail primarily balances the angular momentum of the torso in bipedal hoppers, maintaining a level body pitch during

locomotion. Finally, there exists a specific range of tail masses, as a percentage of total body mass, in which effective bipedal hopping is possible.

In this study, a periodic sinusoidal signal modified by phase offsets controls the animat. This approach allows us to study the morphological characteristics of bipedal hopping with a simple controller reminiscent of a central pattern generator in natural organisms. In future work, we will consider adding an artificial neural network (ANN) controller and expanding the scope of morphological evolution to further investigate bipedal hopping and its associated evolutionary pressures. Adding an ANN might produce gaits not seen here. Additionally, opening other aspects of morphology to evolutionary pressures by adding genes for the dimensions of limbs and torso, joint ranges of motion, and initial position of body components expands the search space considerably. In this study, we intentionally limited the scope of evolvable morphology to the tail length and torso mass in order to focus on the influence of the tail, while maintaining the dimensions of our model organism (*D. deserti*).

6 Source Code

Source code for reproducing the experiments and figures presented in this article is available at https://github.com/jaredmoore/Artificial_Life_Bipedal_Hopping.

Acknowledgments

We would like to acknowledge our funding sources, the Institutional Development Award (IDeA) from the National Institute of General Medical Sciences of the National Institutes of Health under grant P20GM103408, the Army Research Office under 66554-EG, and the NSF-sponsored BEACON Center at Michigan State University.

References

1. Alexander, R., & Vernon, A. (1975). The mechanics of hopping by kangaroos (Macropodidae). *Journal of Zoology*, *177*(2), 265–303.
2. Bennett, M. B. (1987). Fast locomotion of some kangaroos. *Journal of Zoology*, *212*(3), 457–464.
3. Biewener, A., Alexander, R. M., & Heglund, N. C. (1981). Elastic energy storage in the hopping of kangaroo rats (*Dipodomys spectabilis*). *Journal of Zoology*, *195*(3), 369–383.
4. Biewener, A., & Baudinette, R. (1995). In vivo muscle force and elastic energy storage during steady-speed hopping of tammar wallabies (*Macropus eugenii*). *Journal of Experimental Biology*, *198*(9), 1829–1841.
5. Bongard, J. C. (2011). Morphological and environmental scaffolding synergize when evolving robot controllers. In N. Krasnogor (Ed.), *Proceedings of the 13th Annual Conference on Genetic and Evolutionary Computation* (pp. 179–186). New York: ACM.
6. Brooks, R. A. (1992). Artificial life and real robots. In F. Varela & P. Bourgine (Eds.), *Proceedings of the First European Conference on Artificial Life* (pp. 3–10). Cambridge, MA: MIT Press.
7. Clark, A. J., Moore, J. M., Wang, J., Tan, X., & McKinley, P. K. (2012). Evolutionary design and experimental validation of a flexible caudal fin for robotic fish. In C. Adami, D. Bryson, C. Ofria, & R. T. Pennock (Eds.), *Proceedings of the 13th International Conference on the Simulation and Synthesis of Living Systems* (pp. 325–332). Cambridge, MA: MIT Press.
8. Clune, J., Beckmann, B. E., Ofria, C., & Pennock, R. T. (2009). Evolving coordinated quadruped gaits with the HyperNEAT generative encoding. In P. Haddow (Ed.), *Proceedings of the IEEE Congress on Evolutionary Computation* (pp. 2764–2771). Piscataway, NJ: IEEE.
9. DeJong, K. A. (2006). *Evolutionary computation: A unified approach*. Cambridge, MA: MIT Press.
10. Hase, K., Khang, G., & Eom, G.-M. (2004). A simulation study on the evolution of hopping motions in animals. *IEEE Transactions on Systems, Man, and Cybernetics, Part C: Applications and Reviews*, *34*(3), 353–362.
11. Holland, J. H. (1973). Genetic algorithms and the optimal allocation of trials. *SIAM Journal of Computing*, *2*, 88–105.

12. Ijspeert, A. J. (2008). Central pattern generators for locomotion control in animals and robots: A review. *Neural Networks*, *21*(4), 642–653.

13. Jusufi, A., Goldman, D. I., Revzen, S., & Full, R. J. (2008). Active tails enhance arboreal acrobatics in geckos. *Proceedings of the National Academy of Sciences of the U.S.A.*, *105*(11), 4215–4219.

14. Libby, T., Moore, T. Y., Chang-Siu, E., Li, D., Cohen, D. J., Jusufi, A., & Full, R. J. (2012). Tail-assisted pitch control in lizards, robots and dinosaurs. *Nature*, *481*(7380), 181–184.

15. McGowan, C. P., & Collins, C. E. (2018). Why do mammals hop? Understanding the ecology, biomechanics and evolution of bipedal hopping. *The Journal of Experimental Biology*, *221*(12).

16. Moore, J. M., Gutmann, A. K., McGowan, C. P., & McKinley, P. K. (2013). Exploring the role of the tail in bipedal hopping through computational evolution. In P. Lio, O. Miglino, G. Nicosia, S. Nolfi, & M. Pavone (Eds.), *Proceedings of the 12th European Conference on Artificial Life* (pp. 11–18). Cambridge, MA: MIT Press.

17. Sims, K. (1994). Evolving virtual creatures. In S. Mair (Ed.), *Proceedings of the 21st Annual Conference on Computer Graphics and Interactive Techniques* (pp. 15–22). New York: ACM.

18. Smith, R. (2013). Open dynamics engine. http://www.ode.org/.

19. Usherwood, J. R., & Hubel, T. Y. (2012). Energetically optimal running requires torques about the centre of mass. *Journal of the Royal Society Interface*, *9*(73), 2011–2015.

20. Wilson, S. W. (1986). Adaptive and learning systems: Theory and applications. In K. S. Narendra (Ed.), *Adaptive and learning systems: Theory and applications* (pp. 255–264). Boston, MA: Springer US.